metals

MDPI

Article

Dynamic Recovery and Superelasticity of Columnar-Grained Cu–Al–Mn Shape Memory Alloy

Sheng Xu [1,2], Haiyou Huang [1], Jianxin Xie [1,*], Yuta Kimura [2], Xiao Xu [2], Toshihiro Omori [2] and Ryosuke Kainuma [2,*]

1 Key Laboratory for Advanced Materials Processing of the Ministry of Education, University of Science and Technology Beijing, Beijing 100083, China; xu.sheng@hotmail.com (S.X.); huanghy@mater.ustb.edu.cn (H.H.)

2 Department of Materials Science, Graduate School of Engineering, Tohoku University, Sendai 980-8579, Japan; yuta.kimura.s8@dc.tohoku.ac.jp (Y.K.); xu@material.tohoku.ac.jp (X.X.); omori@material.tohoku.ac.jp (T.O.)

* Correspondence: jxxie@mater.ustb.edu.cn (J.X.); kainuma@material.tohoku.ac.jp (R.K.); Tel.: +86-010-6233-2254 (J.X.); +81-022-7957-323 (R.K.)

Academic Editor: Takuo Sakon
Received: 23 March 2017; Accepted: 11 April 2017; Published: 15 April 2017

Abstract: The columnar-grained $Cu_{71.5}Al_{17.5}Mn_{11}$ shape memory alloy was treated by single-pass hot rolling at 900 °C with a thickness reduction of 67.3% followed by immediate water quenching. Dynamic recovery other than discontinuous dynamic recrystallization occurred during the treatment process, bringing about retained columnar grains with <001> textures, as well as dislocations introduced into the parent matrix. As a result, a large maximum recoverable strain of more than 11% was maintained due to the retained beneficial grain characteristics. The critical stress for inducing martensitic transformation and stress hysteresis were enhanced mainly due to the existence of dislocations.

Keywords: shape memory alloy; Cu–Al–Mn; columnar grain; hot deformation; dynamic recovery; martensitic transformation; superelasticity

1. Introduction

Shape memory alloys (SMAs) undergo reversible martensitic phase transformation in response to changes in temperature or applied stress, and hence have unique properties known as the shape memory effect and superelasticity [1,2]. Despite the availability of a commercial Ni–Ti alloy, Cu-based SMAs are the most attractive for practical applications owing to their low cost and good shape memory properties, as well as advantages with regard to electrical and thermal conductivities [1,3].

The shape memory properties of Cu-based SMAs are significantly influenced by their microstructure. Specifically, large grain size and <001> textures are preferred for enhanced superelasticity [4,5]. Recently, directional solidification has been demonstrated to be an effective way for the fabrication of high-performance Cu-based SMAs due to the formation of columnar grains with <001> textures [6–8]. Directionally solidified Cu-based SMAs can be used directly. Sometimes, however, the solidified Cu-based SMAs must undergo plastic processing for different product shapes required for various applications. In this case, two problems are encountered. First, Cu-based SMAs such as Cu–Al–Ni and Cu–Zn–Al are generally too brittle to be sufficiently cold-worked due to the high degree of order in the parent phase and the high elastic anisotropy [1]; thus currently, they can only be used in a solidified state. Second, Cu–Al–Mn SMAs is more ductile than Cu–Al–Ni and Cu–Zn–Al due to a lower degree of order in the parent phase. Therefore, conventional thermomechanical treatment, i.e., cold working and annealing, can be applied to Cu–Al–Mn for plastic processing [3,4,9]. However,

the finally obtained {112} <110> recrystallization texture is not the most favorable texture for obtaining ideal superelastic behavior [4,9]. In a word, it is still difficult to plastically process the solidified Cu-based SMAs without the loss of good superelastic behavior.

When a solidified alloy is subjected to hot deformation, dynamic recovery and discontinuous dynamic recrystallization are involved, the former one usually occurring prior to the latter one [10]. However, it has been found that the dynamic recovery other than discontinuous dynamic recrystallization is preferred to occur for columnar-grained Cu-based alloys during hot deformation, especially when the deformation is perpendicular to the solidification direction (SD) [11,12]. Therefore, in this study, we conducted hot deformation for plastic processing of a columnar-grained Cu–Al–Mn SMA, expecting good superelastic behavior by retention of the beneficial grain characteristics via dynamic recovery.

2. Materials and Methods

A $Cu_{71.5}Al_{17.5}Mn_{11}$ alloy ingot with a columnar-grained microstructure was prepared by directional solidification using homemade equipment. The fabrication process is schematically shown in Figure 1a, and the details can be found in a previous study [7]. The volume of the fabricated ingot was around 150 mm × 80 mm × 40 mm. Dog-bone shaped tensile samples with a gauge size of 20 mm × 4 mm × 1 mm were cut out using wire electro-discharge machining with their longitudinal direction paralleling to SD. These samples were solution-treated (ST) at 800 °C for 5 min followed by quenching in water to obtain a single β_1 phase ($L2_1$ structure) [3], hereafter notated as the as-ST samples. Plates with a size of 50 mm × 15 mm × 5.5 mm were also cut out from the ingot for hot rolling with their longitudinal direction paralleling to SD. These plates were first heated to 900 °C with a holding time of 5 min and subsequently hot-rolled with a twin roller by single pass followed by immediate quenching in water. The diameter of the roller was 200 mm and the rolling speed was set to be 2.0 m/min. The final thickness of the plates after rolling was 1.8 mm with a reduction ratio of 67.3%. The above thermomechanical process, hereafter notated as SHRQ treatment, is illustrated in Figure 1b. Dog-bone shaped tensile samples with a gauge area of 20 mm × 4 mm were then cut out from the hot-rolled plates with their longitudinal direction parallel the rolling direction (RD), hereafter notated as the SHRQ-treated samples.

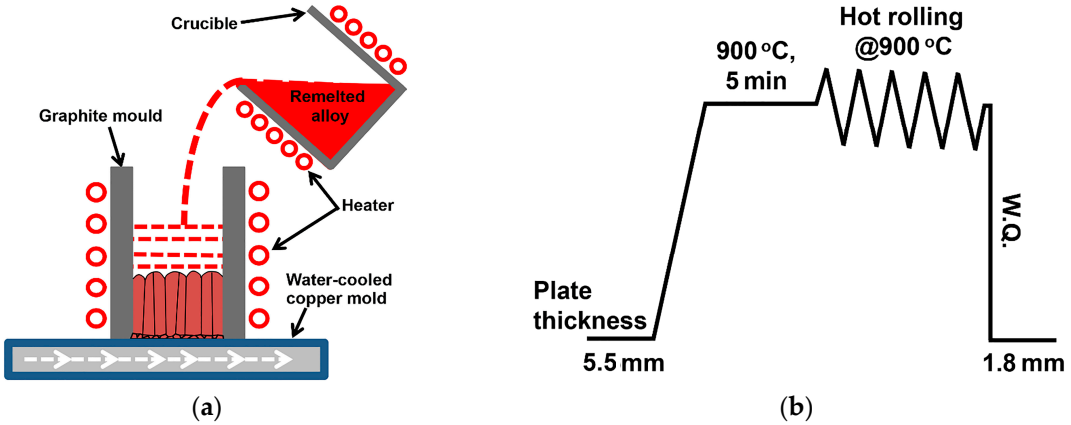

Figure 1. (**a**) Schematic illustration of the directional solidification process. (**b**) Overview of the single-pass hot rolling followed by immediate water quenching (SHRQ) treatment process.

The superelastic response was examined by a cyclic loading–unloading tensile test with increasing applied strain at room temperature with a strain rate of 4.2×10^{-4} s^{-1}. A non-contact video extensometer was used to measure the strain. The crystallographic orientations of the as-ST and SHRQ-treated samples were examined by electron backscattered diffraction (EBSD) employing a field-emission scanning electron microscope (SEM) operated at 20 kV. EBSD samples were finally

polished using a colloidal silica suspension with particle size of 0.04 μm. The martensitic transformation temperatures were determined by the differential scanning calorimetry (DSC) with a heating/cooling rate of 10 °C/min. The crystal structure was analyzed by X-ray diffraction (XRD) method employing Cu Kα radiation at 40 kV with a 2θ angle ranging from 20° to 80°. The microstructure was also observed by using transmission electron microscopy (TEM) operated at 200 kV at room temperature, and the TEM samples were prepared by twin jetting with an electrolyte consisting of 250 mL of H_3PO_4, 50 mL of HCl, 250 mL of C_2H_5OH, 500 mL of distilled water, and 5 g of carbamide.

3. Results and Discussion

Figure 2a,b show the cyclic tensile loading–unloading curves of the as-ST and SHRQ-treated samples at room temperature, respectively. For the as-ST sample, the maximum recoverable strain reaches more than 14%, the critical stress σ_c is 135 MPa, stress hysteresis between forward and reverse transformation is 73 MPa at an applied strain of 13%, where the stress hysteresis is defined as the stress difference between the first loading and unloading curves at half of the applied strain.

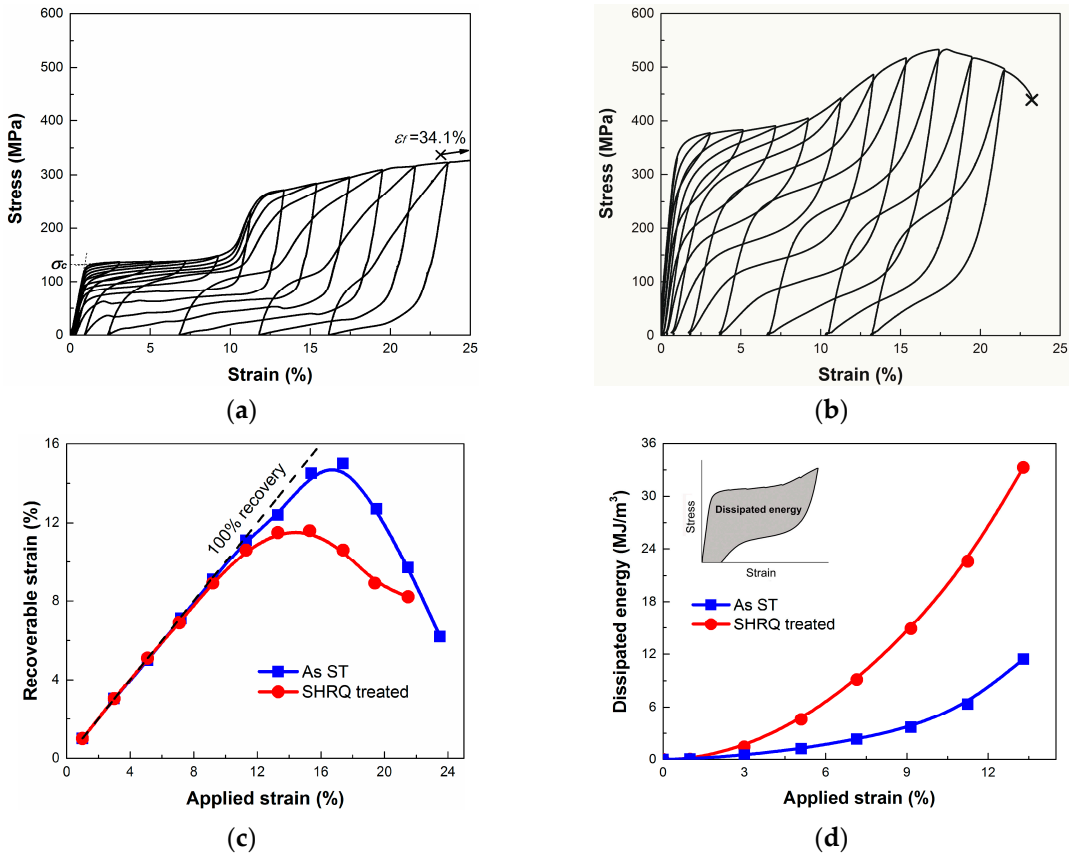

Figure 2. Cyclic tensile stress–strain curves obtained in the (**a**) as-solution-treated (as-ST) sample and (**b**) SHRQ-treated sample at room temperature. (**c**) Recoverable strain as a function of applied tensile strain. (**d**) Mechanical energy dissipated by one superelastic cycle as a function of applied tensile strain for both samples.

For the SHRQ-treated sample, its maximum recoverable strain is maintained at higher than 11%, while the critical stress σ_c is 368 MPa and the stress hysteresis is 254 MPa at an applied strain of 13%, which are 2.7 and 3.5 times as high as those of the as-ST sample, respectively. There is also an increase in apparent Young's modulus after SHRQ treatment. Summarized from Figure 2a,b, the recoverable strain of both samples is plotted against the applied strain in Figure 2c, where the dashed line represents perfect shape recovery. For an applied strain up to 11%, both samples display almost

perfect shape recovery. With a further increase in applied strain, the recovery strain decreases earlier in the SHRQ-treated sample than that of the as-ST sample. Nevertheless, the SHRQ-treated sample still exhibits much better shape recovery properties than that of the ones treated by conventional thermomechanical treatment, in which the maximum recoverable stain is less than 7% [9].

Based on the above results, we can infer that, by using SHRQ treatment, a deformation reduction of 67.3% can be achieved. Meanwhile, the large recoverable strain remained. Moreover, the critical stress σ_c and the stress hysteresis were enhanced, which is potentially important for practical applications of the Cu–Al–Mn SMAs. For example, when SMAs are used as damping vibration components, high critical stress σ_c and stress hysteresis, together with a large recoverable strain, are usually required for a strong damping capacity ΔW, which can be characterized by the enclosed area of the superelastic curves [13,14], as illustrated in the inset of Figure 2d. We made a comparison of damping capacity ΔW in one superelastic cycle at every strain level between the as-ST and SHRQ-treated samples, as shown in Figure 2d. With the increase in applied strain, the ΔW of both samples increases gradually; when the applied strain is 11%, the ΔW of SHRQ-treated sample reaches 22.6 MJ/m^3, which is 3.5 times higher than 6.4 MJ/m^3 in the as-ST sample; when the applied strain is up to 13%, the ΔW of the SHRQ-treated sample reaches 33.3 MJ/m^3, which is 2.9 times higher than the ΔW of the as-ST sample.

As described previously, the superelastic strain of the Cu–Al–Mn SMAs has a strong dependence on microstructure [4,5]. The strong <001> texture and straight grain morphology are the key factors making columnar-grained Cu–Al–Mn alloy show a high recoverable strain [6]. Figure 3a, Figure 4a show the EBSD map and corresponding inverse pole figure of the as-ST sample. It shows a strong <001> texture and straight grain boundaries along the SD, which are typical characteristics of columnar-grained microstructure, and the grain orientations perpendicular to the SD are distributed randomly between <001> and <101> [6]. After SHRQ treatment, even though there was a little loss of orientation uniformity within each separated grain, the <001> texture along the RD was retained, and no recrystallized grain was observed, with the grains in a columnar morphology, as shown in Figure 3b, Figure 4b. The theoretically calculated maximum superelastic strain caused by reversible $\beta_1/6$ M martensitic transformation with stressing along different grain orientations is drawn as contour lines in the inverse pole figure in Figure 3c, Figure 4b [9]. It can be seen that the corresponding theoretical superelastic strain is basically larger than 9% in the SHRQ-treated sample. Therefore, the maintaining of a high recoverable strain in the SHRQ-treated sample is ascribed to the retained <001> texture and columnar grain morphology.

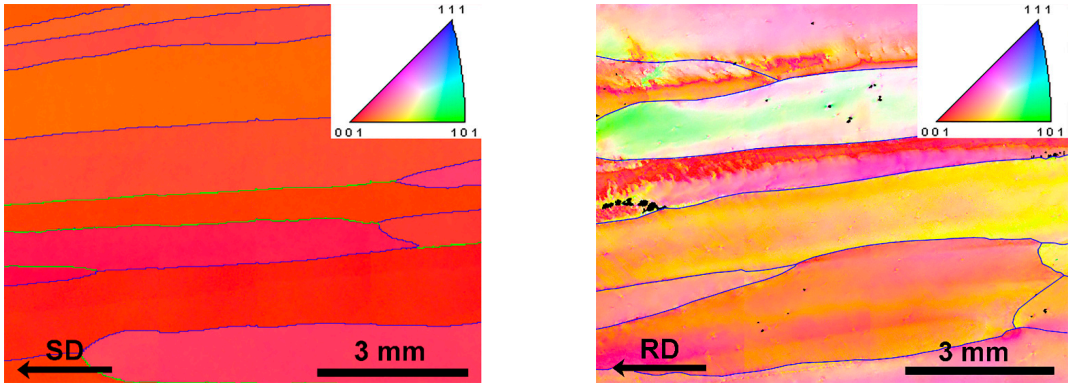

(**a**) (**b**)

Figure 3. Quasi-colored orientation mapping of the (**a**) as-ST sample and the (**b**) SHRQ-treated sample, where the blue line represents a high-angle grain boundary and the green line represents a low-angle grain boundary lower than 15°.

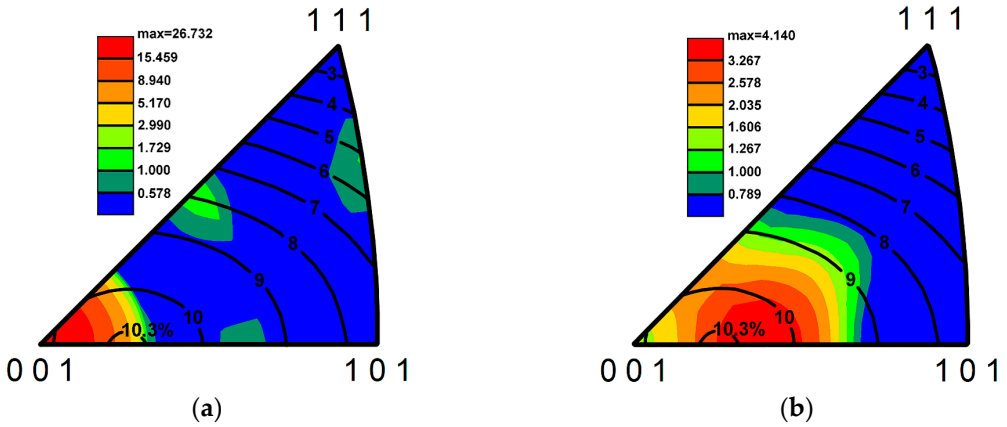

Figure 4. Inverse pole figures with theoretical superelastic strain contour lines of the (**a**) as-ST sample and (**b**) SHRQ-treated sample [9].

It should also be noted that the texture shows a small orientation deviation away from <001> after SHRQ treatment, which probably causes the increase in apparent Young's modulus because the elastic anisotropy is very high in Cu-based SMAs and the Young's modulus along <001> is usually the minimum one [1]. Moreover, the lower intensity of texture after SHRQ treatment should make grain constraint from neighboring grains increase, which may result in an additional increase of Young's modulus. It is also known that the Cu–Al–Mn SMAs display the lowest Tailor factor for the <001> orientation [4]. Therefore, the deviation and weakening of texture for the SHRQ-treated sample should also yield an increase in critical stress σ_c as well as stress hysteresis due to the grain constraint effect [4]. However, even compared with an equiaxed polycrystalline counterpart [9], the critical stress σ_c and stress hysteresis are much higher in the SHRQ-treated sample, which should be caused by other factors.

To further clarify the reasons for the enhanced critical stress σ_c and stress hysteresis, we observed the microstructure of the SHRQ-treated sample by TEM, with Figure 5a showing the TEM bright-field image and corresponding selected area electron diffraction pattern (SAEDP), respectively. It was found that many dislocation distribute in the alloy matrix. The corresponding SAEDP demonstrates that the matrix is the parent phase with a $L2_1$ crystallographic structure. Moreover, no martensite was observed, which is also verified by the XRD pattern, as shown in Figure 5b. It can be inferred then that SHRQ treatment did not introduce residual stress-induced martensite but dislocations into the parent phase. These pre-existing dislocations may have played a key role for the enhanced critical stress σ_c and stress hysteresis in the SHRQ-treated sample, as discussed later.

The thermoelastic martensite in Cu-based SMAs is induced by lowering the temperature or applying stress. The relationship of these two factors for inducing martensitic transformation can be explained by the Clausius–Clapeyron equation [15]:

$$\frac{d\sigma_c}{dT} = -\frac{\Delta S}{\varepsilon \cdot V_m'} \quad (1)$$

where ΔS is the molar entropy change between the parent phase and martensite, ε is the transformation strain, and V_m is the molar volume. In a thermo-induced martensitic transformation, the lower martensitic transformation starting temperature M_s indicates a more stable parent phase, which corresponds to a higher critical stress σ_c in the stress-induced martensitic transformation. It is well known that, for a given chemical composition, the depression of thermo-induced martensitic transformation can be induced by imperfections (dislocations, second-phase particles, precipitates, etc.) [16]. We conducted DSC measurement to determine the martensitic transformation temperatures of both samples, as shown in Figure 5c. The martensitic transformation starting and finishing points M_s, M_f, and the reverse transformation starting and finishing points A_s, and A_f for the as-ST sample are −55.9 °C, −67.6 °C, −51.6 °C, and −39.6 °C, respectively.

Using $d\sigma_c/dT$ = 1.85 MPa/°C for a columnar-grained Cu–Al–Mn SMA [17], the critical stress σ_c at room temperature is calculated to be around 140 MPa for the as-ST sample, which is consistent with the experimental value of 135 MPa. However, no martensitic transformation is observed for the SHRQ-treated sample, even cooled down to 80 °C, indicating that the parent phase was stabilized due to the existence of dislocations strongly hindering the nucleation of martensite, and therefore the M_s was greatly depressed. In addition, it is also known that a lower degree of order in the parent phase results in a decrease in M_s in the Cu–Al–Mn SMA [18]. By comparing the ratio of the intensities (I) between (200) and (400) peaks for both samples using the XRD patterns in Figure 5b, i.e., $I_{(200)}/I_{(400)}$, a lower degree of order for the SHRQ-treated sample can be verified due to a lower value of $I_{(200)}/I_{(400)}$, which may also give a decrease in M_s and subsequent increase in critical stress σ_c at room temperature.

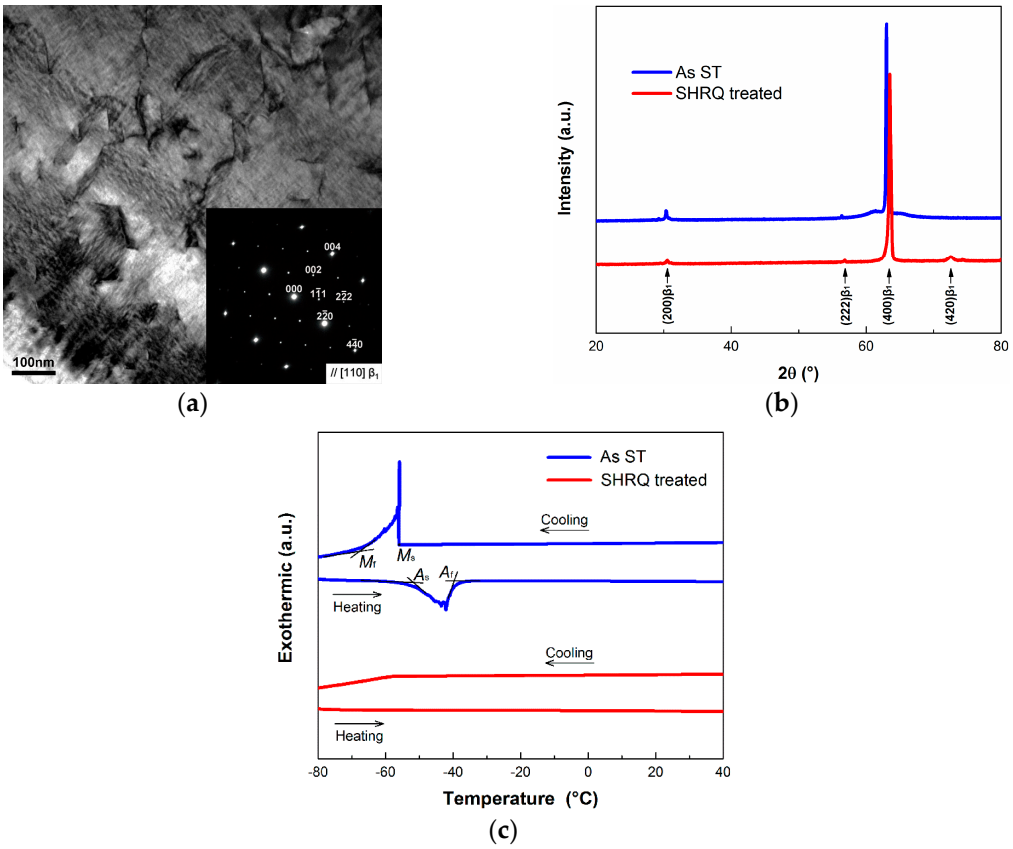

Figure 5. (**a**) TEM bright-field image of the SHRQ-treated sample showing dislocations distributed in the matrix, the inset shows the selected area electron diffraction pattern of the matrix. (**b**) XRD patterns and (**c**) DSC curves of the as-ST sample and SHRQ-treated sample.

For SMAs, the stress hysteresis is generally affected by friction against migration of parent/martensite interfaces and dislocation generation. [19,20]. The intrinsic interface friction is usually dominated by the lattice incompatibility between transforming phases, which is mainly related to the chemical composition. In our case, the SHRQ treatment did not change the chemical composition of the alloy, so the increase in stress hysteresis in the SHRQ-treated sample should be attributed to the dislocations introduced into the parent phase accordingly. The pre-existing dislocations in the parent phase have already been demonstrated to improve stress hysteresis by hindering the growth of martensite by impeding the motion of parent phase/martensite interfaces [21]. Therefore, it is apparent that the dislocations introduced into the non-martensite parent phase by SHRQ treatment significantly enhanced the stress hysteresis.

4. Conclusions

In conclusion, with single-pass hot rolling followed by immediate water quenching treatment, a plastic reduction of 67.3% was achieved in the columnar-grained $Cu_{71.5}Al_{17.5}Mn_{11}$ shape memory alloy. Meanwhile, a large maximum recoverable strain of more than 11%, as well as enhanced critical stress σ_c and stress hysteresis were obtained. The retained columnar grains with <001> textures due to dynamic recovery during treatment were believed to be the reasons for the maintenance of a high recoverable strain. The dislocations introduced into the parent matrix served mainly for enhancing the critical stress σ_c and stress hysteresis. This study should be useful in further improvement in the plastically processing the solidified brittle Cu-based shape memory alloys while maintaining good superelastic behavior at the same time.

Acknowledgments: This work was financially supported by the National Natural Science Foundation of China (Grant No. 51574027), the National Key Research and Development Program of China (Grant No. 2016YFB0700505), and the Discipline Innovative Engineering Plan of China (111 Project) (Grant No. B17003).

Author Contributions: Sheng Xu, Haiyou Huang, and Xiao Xu conceived and designed the experiments; Sheng Xu performed the experiments; Sheng Xu and Haiyou Huang analyzed the data, and wrote the paper; Yuta Kimura conducted the TEM experiments; Jianxin Xie, Xiao Xu, Toshihiro Omori and Ryosuke Kainuma supported the paper writing. All authors have participated in the discussions of the results.

Conflicts of Interest: The authors declare no conflict of interest.

References

1. Otsuka, O.; Wayman, C.M. *Shape Memory Materials*, 1st ed.; Cambridge University Press: Cambridge, UK, 1998; pp. 97–116.
2. Juan, J.S.; Nó, M.L.; Schuh, C.A. Nanoscale shape-memory alloys for ultrahigh mechanical damping. *Nat. Nanotechnol.* **2009**, *4*, 415–419. [CrossRef] [PubMed]
3. Sutou, Y.; Omori, T.; Kainuma, R.; Ishida, K. Ductile Cu–Al–Mn shape memory alloys: General properties and applications. *Mater. Sci. Technol.* **2008**, *24*, 896–901. [CrossRef]
4. Sutou, Y.; Omori, T.; Yamauchi, K.; Ono, N.; Kainuma, R.; Ishida, K. Effect of grain size and texture on pseudoelasticity in Cu–Al–Mn-based shape memory wire. *Acta Mater.* **2005**, *53*, 4121–4133. [CrossRef]
5. Sutou, Y.; Omori, T.; Kainuma, R.; Ishida, K. Grain size dependence of pseudoelasticity in polycrystalline Cu–Al–Mn-based shape memory sheets. *Acta Mater.* **2013**, *61*, 3842–3850. [CrossRef]
6. Liu, J.L.; Huang, H.Y.; Xie, J.X. The roles of grain orientation and grain boundary characteristics in the enhanced superelasticity of $Cu_{71.8}Al_{17.8}Mn_{10.4}$ shape memory alloys. *Mater. Des.* **2014**, *64*, 427–433. [CrossRef]
7. Liu, J.L.; Huang, H.Y.; Xie, J.X. Superelastic anisotropy characteristics of columnar-grained Cu–Al–Mn shape memory alloys and its potential applications. *Mater. Des.* **2015**, *85*, 211–220. [CrossRef]
8. Fu, H.D.; Song, S.; Zhuo, L.; Zhang, Z.H.; Xie, J.X. Enhanced mechanical properties of polycrystalline Cu–Al–Ni alloy through grain boundary orientation and composition control. *Mater. Sci. Eng. A* **2016**, *650*, 218–224. [CrossRef]
9. Sutou, Y.; Omori, T.; Kainuma, R.; Ono, N.; Ishida, K. Enhancement of superelasticity in Cu–Al–Mn-Ni shape-memory alloys by texture control. *Metall. Mater. Trans. A* **2002**, *22*, 2814–2824. [CrossRef]
10. Humphreys, F.J.; Hatherly, M. *Recrystallization and Related Annealing Phenomena*, 2nd ed.; Elsevier: Oxford, UK, 2004; pp. 415–437.
11. Yu, J.; Liu, X.; Xie, J. Study on dynamic recrystallization of a Cu-based alloy BFe10-1-1 with continuous columnar grains. *Acta Metall. Sin.* **2011**, *47*, 482–488.
12. Liu, Y.K.; Huang, H.Y.; Xie, J.X. Effect of compression direction on the dynamic recrystallization behavior of continuous columnar-grained $CuNi_{10}Fe_1Mn$ alloy. *Int. J. Miner. Mater. Metall.* **2015**, *28*, 851–859. [CrossRef]
13. Ma, J.; Karaman, I. Expanding the repertoire of shape memory alloy. *Science* **2010**, *327*, 1468–1469. [CrossRef] [PubMed]
14. Tanaka, Y.; Himuro, Y.; Kainuma, R.; Sutou, Y.; Ishida, K. Ferrous polycrystalline shape-memory alloy showing huge superelasticity. *Science* **2010**, *327*, 1488–1490. [CrossRef] [PubMed]

15. Wollants, P.; Bonte, M.D.; Roos, J.R. Thermodynamic analysis of the stress-induced martensitic transformation in a single crystal. *Z. Metallk.* **1979**, *70*, 113–117.
16. Sutou, Y.; Koeda, N.; Omori, T.; Kainuma, R.; Ishida, K. Effect of aging on bainitic and thermally induced martensitic transformations in ductile Cu–Al–Mn-based shape memory alloys. *Acta Mater.* **2009**, *57*, 5748–5758. [CrossRef]
17. Xu, S.; Huang, H.Y.; Xie, J.; Takekawa, S.; Xu, X.; Omori, T.; Kainuma, R. Giant elastocaloric effect covering wide temperature range in columnar-grained $Cu_{71.5}Al_{17.5}Mn_{11}$ shape memory alloy. *APL Mater.* **2016**, *4*, 106106. [CrossRef]
18. Kainuma, R.; Takahashi, S.; Ishida, K. Ductile shape memory alloys of the Cu–Al–Mn system. *J. Phys. IV* **1995**, *5*, 961–966. [CrossRef]
19. Ortín, J.; Planes, A. Thermodynamic analysis of thermal measurements in thermoelastic martensitic transformations. *Acta Metall.* **1988**, *36*, 1873–1889. [CrossRef]
20. Karaca, H.E.; Acar, E.; Basaran, B.; Noebe, R.D.; Chumlyakov, Y.I. Superelastic response and damping capacity of ultrahigh-strength [111]-oriented NiTiHfPd single crystals. *Scri. Mater.* **2012**, *67*, 447–450. [CrossRef]
21. Romero, R.; Lovey, F.C.; Ahlers, M. The effect of β phase plastic deformation on martensitic transformation in Cu–Zn and Cu–Zn–Al single crystals. *Scri. Metall.* **1990**, *24*, 285–289. [CrossRef]

© 2017 by the authors. Licensee MDPI, Basel, Switzerland. This article is an open access article distributed under the terms and conditions of the Creative Commons Attribution (CC BY) license (http://creativecommons.org/licenses/by/4.0/).